MIT Libraries | DSpace@MIT

MIT Open Access Articles

Joint generative model for fMRI/ DWI and its application to population

The MIT Faculty has made this article openly available. ***Please share*** how this access benefits you. Your story matters.

Citation: Hutchison, David et al. "Joint Generative Model for fMRI/DWI and Its Application to Population Studies." Medical Image Computing and Computer-Assisted Intervention – MICCAI 2010. Ed. Tianzi Jiang et al. LNCS Vol. 6361. Berlin, Heidelberg: Springer Berlin Heidelberg, 2010. 191–199.

As Published: http://dx.doi.org/10.1007/978-3-642-15705-9_24

Publisher: Springer Berlin / Heidelberg

Persistent URL: http://hdl.handle.net/1721.1/74083

Version: Author's final manuscript: final author's manuscript post peer review, without publisher's formatting or copy editing

Terms of use: Creative Commons Attribution-Noncommercial-Share Alike 3.0

Massachusetts Institute of Technology

NIH Public Access
Author Manuscript
Med Image Comput Comput Assist Interv. Author manuscript; available in PMC 2011 March 12.

Published in final edited form as:
Med Image Comput Comput Assist Interv. 2010 ; 13(Pt 1): 191–199.

Joint Generative Model for fMRI/DWI and Its Application to Population Studies

Archana Venkataraman[1], **Yogesh Rathi**[2], **Marek Kubicki**[2], **Carl-Fredrik Westin**[3,1], and **Polina Golland**[1]

[1] MIT Computer Science and Artificial Intelligence Laboratory, Cambridge, MA

[2] Psychiatry Neuroimaging Laboratory, Harvard Medical School, Boston, MA

[3] Laboratory for Mathematics Imaging, Harvard Medical School, Boston, MA

Abstract

We propose a novel probabilistic framework to merge information from DWI tractography and resting-state fMRI correlations. In particular, we model the interaction of *latent* anatomical and functional connectivity templates between brain regions and present an intuitive extension to population studies. We employ a mean-field approximation to fit the new model to the data. The resulting algorithm identifies differences in latent connectivity between the groups. We demonstrate our method on a study of normal controls and schizophrenia patients.

1 Introduction

The interaction between functional and anatomical connectivity provides a rich framework for understanding the brain. Functional connectivity is commonly measured via temporal correlations in resting-state fMRI data. These correlations are believed to reflect the intrinsic functional organization of the brain [1]. Anatomical connectivity is often measured using DWI tractography which estimates the configuration of underlying white matter fibers [2]. In this work we propose and demonstrate a novel probabilistic framework to infer the relationship between these modalities. The model is based on *latent* connectivities between brain regions and makes intuitive assumptions about the data generation process. We present a natural extension of the model to population studies, which we use to identify widespread connectivity changes in schizophrenia.

To date, relatively little progress has been made in fusing information between the aforementioned anatomical and functional modalities. It has been shown that while a high degree of structural connectivity predicts higher functional correlations, the converse does not always hold [3,4]. For example, strong functional correlations can be found between spatially distributed locations in the brain. However, one is more likely to identify white matter tracts connecting nearby regions. Graph-theoretic models have previously been used to examine the correspondence between independently estimated structural hubs and functional networks [5,6]. In contrast, we infer a population template of connectivity using *both* resting-state fMRI correlations and DWI tractography.

We demonstrate the capability of our model to learn stable patterns on a population study of schizophrenia. Schizophrenia is a poorly-understood disorder marked by widespread cognitive difficulties affecting intelligence, memory, and executive attention. These impairments are not localized to a particular cortical region; rather, they reflect

NIH-PA Author Manuscript
NIH-PA Author Manuscript
NIH-PA Author Manuscript

NIH-PA Author Manuscript

NIH-PA Author Manuscript

NIH-PA Author Manuscript

abnormalities in widely-distributed functional and anatomical networks [7,8]. In accordance with these findings, our model identifies connectivity differences in spatially extensive networks.

Only a few studies to date have combined resting-state fMRI and DWI tractography to analyze schizophrenia [9,10]. Univariate statistical tests are commonly used to identify significant population differences in temporal correlations and in mean Fractional Anisotrophy (FA) values. The relevant connections are then compared across modalities to draw conclusions. This approach treats functional and structural connections as *a priori* independent and ignores distributed patterns of connectivity. In contrast, our model jointly infers the entire pattern of functional and anatomical connectivity, as well as the group differences.

2 Generative Model and Inference

Unlike voxel- and ROI-based analysis, we model the behavior of *pairwise connections* between regions of the brain. Our observed variables are correlations in resting-state fMRI and average FA values along the white matter tracts.

Latent Connectivity

Fig. 1(a) shows our model for a single population. Let N be the total number of relevant connections in the brain. A_n and F_n are the latent anatomical and functional connectivity measures between the two regions associated with the n^{th} connection. A_n is a binary random variable with parameter π_A: $P(A_n;\pi_A) = \pi_A^{A_n}(1-\pi_A)^{1-A_n}$. It indicates the presence or absence of a *direct* anatomical pathway between the regions. In contrast, F_n is a tri-state random variable drawn from a multinomial distribution π_F. These states represent little or no functional co-activation ($F_n = 0$), positive functional synchrony ($F_n = 1$), and negative functional synchrony ($F_n = -1$) between the regions. For notational convenience, we represent F_n as a length-three indicator vector with exactly one of its elements $\{F_{nk} : k = -1, 0, 1\}$ equal to one:

$$P(F_n;\pi_F) = \prod_{k=-1}^{1} (\pi_{Fk})^{F_{nk}}. \tag{1}$$

Data Likelihood

Let J be the number of subjects. The DWI measurement D_n^j for the j^{th} subject is a noisy observation of the anatomical connectivity A_n:

$$P\left(\mathrm{D}_n^j \middle| A_n; \{\rho, \chi, \xi\}\right) = \left[\rho_0 \delta\left(\mathrm{D}_n^j\right) + (1-\rho_0)\,\mathcal{N}\left(\mathrm{D}_n^j; \chi_0, \xi_0^2\right)\right]^{(1-A_n)} \cdot \left[\rho_1 \delta\left(\mathrm{D}_n^j\right) + (1-\rho_1)\,\mathcal{N}\left(\mathrm{D}_n^j; \chi_1, \xi_1^2\right)\right]^{A_n}, \tag{2}$$

where $\delta(\cdot)$ is the Dirac delta function, $N(\cdot; \chi, \xi^2)$ is a Gaussian distribution with mean χ and variance ξ^2, and ρ is the probability of failing to find a tract between two regions. The value zero of D_n^j is arbitrarily chosen to represent "No Connection". D_n^j is strictly positive when a connection is present.

The BOLD fMRI correlation B_n^j for the j^{th} subject depends on both F_n and A_n since direct anatomical connections predict higher functional correlations:

NIH-PA Author Manuscript

NIH-PA Author Manuscript

NIH-PA Author Manuscript

$$P\left(\mathrm{B}_n^j \middle| A_n, F_n; \{\mu, \sigma\}\right) = \prod_{k=-1}^{1} \left[\mathcal{N}\left(\mathrm{B}_n^j; \mu_{0k}, \sigma_{0k}^2\right)^{(1-A_n)} \cdot \mathcal{N}\left(\mathrm{B}_n^j; \mu_{1k}, \sigma_{1k}^2\right)^{A_n} \right]^{F_{nk}} \cdot \tag{3}$$

Using histograms of the data, we verified that the Gaussian distributions in Eqs. (2-3) provide reasonable approximations for the DWI and fMRI data. Pragmatically, they greatly simplify the learning/inference steps.

Population Differences

Fig. 1(b) depicts an extension of the model to a population study involving controls and schizophrenia patients. We model differences between the groups within the latent connectivities alone and share the data likelihood distributions between the two populations.

We treat the latent connectivity templates $\left\{\mathrm{A}_n^S, \mathrm{F}_n^S\right\}$ of the schizophrenia population as "corrupted" versions of the healthy template. In particular, with (small) probability ε, each connection can switch its state:

$$P\left(\mathrm{A}_n^S \middle| \mathrm{A}_n^C; \varepsilon_A\right) = \varepsilon_A^{\mathrm{A}_n^C(1-\mathrm{A}_n^S)+(1-\mathrm{A}_n^C)\mathrm{A}_n^S} \cdot (1-\varepsilon_A)^{\mathrm{A}_n^C\mathrm{A}_n^S+(1-\mathrm{A}_n^C)(1-\mathrm{A}_n^S)}, \tag{4}$$

$$P\left(\mathrm{F}_n^S \middle| \mathrm{F}_n^C; \varepsilon_F\right) = \prod_{k=-1}^{1} \left(\frac{\varepsilon_F}{2}\right)^{(1-\mathrm{F}_{nk}^C\mathrm{F}_{nk}^S)} \cdot (1-\varepsilon_F)^{\mathrm{F}_{nk}^C\mathrm{F}_{nk}^S}. \tag{5}$$

For robustness, we rely on a single scalar to govern the probability of change within each modality. Additionally, in Eq. (5) we assume that functional connectivity switches to its other two states with equal probability.

Variational EM Solution

It is not difficult to show that the complete log-likelihood of all the random variables has multiplicative interactions among the hidden variables. For this reason, we employ the mean-field algorithm [11] to approximate the posterior probability distribution of the latent variables using a fully factorized distribution.

We let $\left\{\widehat{p}_n^C, \widehat{p}_n^S, \widehat{q}_{nk}^C, \widehat{q}_{nk}^S\right\}$ represent the posterior probability estimates for $\left\{\mathrm{A}_n^C, \mathrm{A}_n^S, \mathrm{F}_n^C, \mathrm{F}_n^S\right\}$. The variational EM algorithm alternates between updating the posterior estimates and the model parameters to minimize the variational free energy. Due to space constraints, we directly present the update rules.

Learning—We fix the posterior distributions and learn the model parameters. Let J_n^0 be the number of healthy subjects for which $\mathrm{D}_n^j=0$, and let M_n^0 be similarly defined for schizophrenia patients. The update rules are identical to those of the standard EM. The probability estimates are sums of the latent posteriors:

NIH-PA Author Manuscript

NIH-PA Author Manuscript

NIH-PA Author Manuscript

$$\pi_A = \frac{1}{N}\sum_{n=1}^{N} \widehat{p}_n^C \qquad \pi_{Fk} = \frac{1}{N}\sum_{n=1}^{N} \widehat{q}_{nk}^C$$

$$\varepsilon_A = \frac{1}{N}\sum_{n=1}^{N} \widehat{p}_n^C(1-\widehat{p}_n^S) + (1-\widehat{p}_n^C)\widehat{p}_n^S \qquad \varepsilon_F = 1 - \frac{1}{N}\sum_{n=1}^{N}\sum_{k=-1}^{1} \widehat{q}_{nk}^C \widehat{q}_{nk}^S$$

and the density parameters are equal to weighted statistics of the data:

$$\mu_{1k} = \frac{\sum_{n=1}^{N}\left[\widehat{p}_n^C \widehat{q}_{nk}^C \sum_{j=1}^{J} \mathrm{B}_{nk}^j + \widehat{p}_n^S \widehat{q}_{nk}^S \sum_{m=1}^{M} \mathrm{B}_{nk}^m\right]}{\sum_{n=1}^{N}\left[\widehat{p}_n^C \widehat{q}_{nk}^C J + \widehat{p}_n^S \widehat{q}_{nk}^S M\right]}$$

$$\sigma_{1k}^2 = \frac{\sum_{n=1}^{N}\left[\widehat{p}_n^C \widehat{q}_{nk}^C \sum_{j=1}^{J} \left(\mathrm{B}_{nk}^j - \mu_{1k}\right)^2 + \widehat{p}_n^S \widehat{q}_{nk}^S \sum_{m=1}^{M} \left(\mathrm{B}_{nk}^m - \mu_{1k}\right)^2\right]}{\sum_{n=1}^{N}\left[\widehat{p}_n^C \widehat{q}_{nk}^C J + \widehat{p}_n^S \widehat{q}_{nk}^S M\right]}$$

$$\rho_1 = \frac{\sum_{n=1}^{N}\left[\widehat{p}_n^C J_n^0 + \widehat{p}_n^S M_n^0\right]}{\sum_{n=1}^{N}\left[\widehat{p}_n^C J + \widehat{p}_n^S M\right]} \qquad \chi_1 = \frac{\sum_{n=1}^{N}\left[\widehat{p}_n^C \sum_{j:\mathrm{D}_n^j>0} \mathrm{D}_n^j + \widehat{p}_n^S \sum_{m:\mathrm{D}_n^m>0} \mathrm{D}_n^m\right]}{\sum_{n=1}^{N}\left[\widehat{p}_n^C (J - J_n^0) + \widehat{p}_n^S (M - M_n^0)\right]}$$

$$\xi_1^2 = \frac{\sum_{n=1}^{N}\left[\widehat{p}_n^C \sum_{j:\mathrm{D}_n^j>0} \left(\mathrm{D}_n^j - \chi_1\right)^2 + \widehat{p}_n^S \sum_{m:\mathrm{D}_n^m>0} \left(\mathrm{D}_n^m - \chi_1\right)^2\right]}{\sum_{n=1}^{N}\left[\widehat{p}_n^C (J - J_n^0) + \widehat{p}_n^S (M - M_n^0)\right]}$$

The parameter updates for $\{\mu_{0k}, \sigma_{0k}^2, \rho_0, \chi_0, \xi_0^2\}$ are trivially obtained from these expressions by replacing $\widehat{p}_n^C$ with $\left(1 - \widehat{p}_n^C\right)$ and $\widehat{p}_n^S$ with $\left(1 - \widehat{p}_n^S\right)$.

Inference—We fix the model parameters and update the variational posteriors. We use $\mathcal{P}_l(\cdot)$ to denote the mixture distribution in Eq. (2) and $\mathcal{G}_{lk}(\cdot)$ to denote a normal distribution with parameters $\{\mu_{lk}, \sigma_{lk}\}$ in order to obtain:

$$\frac{\widehat{p}_n^C}{1-\widehat{p}_n^C} = \left(\frac{\pi_A}{1-\pi_A}\right)\left(\frac{1-\varepsilon_A}{\varepsilon_A}\right)^{(2\widehat{p}_n^S - 1)} \prod_{j=1}^{J}\left(\frac{\mathcal{P}_1(\mathrm{D}_n^j)}{\mathcal{P}_0(\mathrm{D}_n^j)}\right) \prod_{k=-1}^{1}\left(\frac{\mathcal{G}_{1k}(\mathrm{B}_n^j)}{\mathcal{G}_{0k}(\mathrm{B}_n^j)}\right)^{\widehat{q}_{nk}^C}$$

$$\frac{\widehat{p}_n^S}{1-\widehat{p}_n^S} = \left(\frac{1-\varepsilon_A}{\varepsilon_A}\right)^{(2\widehat{p}_n^C - 1)} \prod_{m=1}^{M}\left(\frac{\mathcal{P}_1(\mathrm{D}_n^m)}{\mathcal{P}_0(\mathrm{D}_n^m)}\right) \prod_{k=-1}^{1}\left(\frac{\mathcal{G}_{1k}(\mathrm{B}_n^m)}{\mathcal{G}_{0k}(\mathrm{B}_n^m)}\right)^{\widehat{q}_{nk}^S}$$

$$\widehat{q}_{nk}^C \propto \pi_{Fk} \cdot \left(\frac{1-\varepsilon_F}{(\varepsilon_F/2)}\right)^{\widehat{q}_{nk}^S} \prod_{j=1}^{J}\left(\mathcal{G}_{1k}\left(\mathrm{B}_n^j\right)\right)^{\widehat{p}_n^C}\left(\mathcal{G}_{0k}\left(\mathrm{B}_n^j\right)\right)^{(1-\widehat{p}_n^C)} \quad s.t. \sum_{k=-1}^{1} \widehat{q}_{nk}^C = 1$$

$$\widehat{q}_{nk}^S \propto \left(\frac{1-\varepsilon_F}{(\varepsilon_F/2)}\right)^{\widehat{q}_{nk}^C} \prod_{m=1}^{M}\left(\mathcal{G}_{1k}\left(\mathrm{B}_n^m\right)\right)^{\widehat{p}_n^S}\left(\mathcal{G}_{0k}\left(\mathrm{B}_n^m\right)\right)^{(1-\widehat{p}_n^S)} \quad s.t. \sum_{k=-1}^{1} \widehat{q}_{nk}^S = 1$$

As seen, the updates can be decomposed into a prior term (for normal subjects only), a term arising from the connectivity changes between the populations, and a data likelihood term involving the other modality.

Model Evaluation

Based on the latent posterior probabilities $\{\widehat{p}_n^C, \widehat{p}_n^S, \widehat{q}_{nk}^C, \widehat{q}_{nk}^C\}$, the empirical probability of change in the anatomical or functional connectivity of the n^{th} connection is

NIH-PA Author Manuscript

NIH-PA Author Manuscript

NIH-PA Author Manuscript

$$\widehat{\varepsilon}_A^n = \widehat{p}_n^C\left(1-\widehat{p}_n^S\right)+\left(1-\widehat{p}_n^S\right)\widehat{p}_n^S \quad \text{and} \quad \widehat{\varepsilon}_F^n = 1-\sum_{k=-1}^{1}\widehat{q}_{nk}^C\widehat{q}_{nk}^S \tag{6}$$

respectively. We evaluate the significance and robustness of our model through non-parametric permutation tests and cross-validataion. To construct the distributions for $\widehat{\varepsilon}_A^n$ and $\widehat{\varepsilon}_F^n$ under the null hypothesis, we randomly permute the subject labels (NC vs. SZ) 10, 000 times. For each permutation, we fit the model and compute the relevant statistics in Eq. (6). The significance (p-value) of each connection is equal to the proportion of permutations for which the computed statistic is greater than or equal to the value obtained under the true labeling.

We also quantify the model's predictive power via ten-fold cross validation. The model is fit using the training subjects, and a likelihood ratio test is used to predict the diagnosis for the held-out group. The data is resampled 20 times to ensure stability of the results. For comparison, we perform the same ten-fold cross validation using support vector machine (SVM) classifiers trained on the fMRI correlations, the DWI FA values, and the combined fMRI and DWI data.

3 Results

Data

We demonstrate our model on a study of 18 male patients with chronic schizophrenia and 18 male healthy controls. The control participants were group matched to the patients on age, handedness, parental socioeconomic status, and an estimated premorbid IQ. For each subject, an anatomical scan (SPGR, $TR = 7.4s$, $TE = 3ms$, $FOV = 26cm^2$, $res = 1mm^3$), a diffusion-weighted scan (EPI, $TR = 17s$, $TE = 78ms$, $FOV = 24cm^2$, $res = 1.66 \times 1.66 \times 1.7mm$, 51 gradient directions with $b = 900s/mm^2$, 8 baseline scans with $b = 0s/mm^2$) and a resting-state functional scan (EPI-BOLD, $TR = 3s$, $TE = 30ms$, $FOV = 24cm^2$, $res = 1.875 \times 1.875 \times 3mm$) were acquired using a 3T GE Echospeed system.

Pre-Processing

We segmented the structural images into 77 anatomical regions with Freesurfer [12]. The DWI data was corrected for eddy-current distortions. Two-tensor tractography was used to estimate the white matter fibers [13]. We compute the DWI connectivity D_n^j by averaging FA along *all* fibers connecting the corresponding regions. If no tracts are found, D_n^j is set to zero.

We discarded the first five fMRI time points and performed motion correction by rigid body alignment and slice timing correction using FSL [14]. The data was spatially smoothed using a Gaussian filter, temporally low-pass filtered with $0.08Hz$ cutoff, and motion corrected via linear regression. Finally, we regressed out global contributions to the timecourses from the white matter, ventricles and the whole brain. We extract the fMRI connectivity B_n^j by computing Pearson correlation coefficients between every pair of voxels in the two regions of the n^{th} connection, applying the Fisher-r-to-z transform to each correlation (to enforce normality), and averaging these values. Since our anatomical regions are large, the correlation between the mean timecourses of two regions shows poor correspondence with the distribution of voxel-wise correlations between them. We believe our measure is more appropriate for assessing fMRI connectivity.

NIH-PA Author Manuscript

NIH-PA Author Manuscript

NIH-PA Author Manuscript

To inject prior clinical knowledge, we pre-selected 8 brain structures (corresponding to 16 regions) that are believed to play a role in schizophrenia: the superior temporal gyrus, rostral middle frontal gyrus, hippocampus, amygdala, posterior cingulate, rostral anterior cingulate, parahippocampal gyrus, and transverse temporal gyrus. We model only the $1096\left(16\times 76-\left(\begin{array}{c}16\\2\end{array}\right)\right)$ unique pairwise connections between these ROIs and all other regions in the brain.

Joint Connectivity Model

We first fit the joint model in Fig. 1(a) to each population separately as well as to the entire dataset. Table 1 reports the parameters of the three models. We observe that $\{\mu, \sigma, \rho, \chi, \xi\}$ are largely consistent across the three models. This supports our hypothesis that group differences appear in the latent connectivities rather than in the data likelihood parameters.

Population Study

Fig. 2 depicts the significantly different ($p < 0.05$, $\hat{\varepsilon} > 0.5$) anatomical and functional connections identified by the algorithm. Table 2 lists the corresponding regions and p-values. Due to space limitations, we report just the 3 connections with the smallest p-values in each modality.

As seen from Fig. 2(b), schizophrenia patients exhibit increased functional connectivity between the parietal/posterior cingulate region and the frontal lobe and reduced functional connectivity between the parietal/posterior cingulate region and the temporal lobe. These results confirm the hypotheses of widespread functional connectivity changes in schizophrenia and of functional abnormalities involving the default network.

The differences in anatomical connectivity implicate the superior temporal gyrus and hippocampus. These regions have been cited in prior DTI studies of schizophrenia [15]. We note that relatively few anatomical connections exhibit significant differences between the two populations. This may stem from our choice of ROIs. In particular, we rely on Freesurfer parcellations, which provide anatomically meaningful correspondences across subjects. These larger regions also mitigate the effects of minor registration errors. However, they may be too big to capture structural differences between the groups. We emphasize that our model can be easily applied to finer scale parcelations in future studies.

Table 3 reports classification accuracies for the generative model and SVM classifiers. Despite not being optimized for classification, our model exhibits above-chance generalization accuracy. We note that even the SVM does not achieve high discrimination accuracy. This underscores the well-documented challenge of finding robust functional and anatomical changes induced by schizophrenia [15]. We stress that our main goal is to explain differences in connectivity. Classification is only presented for validation.

4 Conclusion

We proposed a novel probabilistic framework that fuses information from resting-state fMRI data and DWI tractography. We further extended the basic approach to model connectivity differences between two populations. We show that our method captures changes in functional and anatomical connectivity induced by schizophrenia. In particular, we detect increased functional connectivity from the parietal lobe to the frontal lobe and decreased functional connectivity from the parietal lobe to the temporal lobe. We also find significant anatomical connectivity differences involving the superior temporal gyrus, the posterior cingulate and the hippocampus. Finally, we demonstrate the predictive power of our model

NIH-PA Author Manuscript

NIH-PA Author Manuscript

NIH-PA Author Manuscript

through cross validation. These results establish the promise of our approach for combining multiple imaging modalities to better understand the brain.

Acknowledgments

This work was supported in part by the National Alliance for Medical Image Analysis (NIH NIBIB NAMIC U54-EB005149), the Neuroimaging Analysis Center (NIH NCRR NAC P41-RR13218), the NSF CAREER Grant 0642971 and NIH R01MH074794. A. Venkataraman is supported by the National Defense Science and Engineering Graduate Fellowship (NDSEG).

References

1. Buckner RL, Vincent JL. Unrest at rest: Default activity and spontaneous network correlations. NeuroImage 2007;37(4):1091–1096. [PubMed: 17368915]
2. Basser P, Pierpaoli C. Microstructural and physiological features of tissues elucidated by quantitative-diffusion-tensor mri. Journal of Magnetic Resonance, Series B 1996;111:209–219. [PubMed: 8661285]
3. Honey C, et al. Predicting human resting-state functional connectivity from structural connectivity. PNAS 2009;106(6):2035–2040. [PubMed: 19188601]
4. Koch MA, et al. An investigation of functional and anatomical connectivity using magnetic resonance imaging. NeuroImage 2002;16(1):241–250. [PubMed: 11969331]
5. Sporns O, et al. Theoretical neuroanatomy: Relating anatomical and functional connectivity in graphs and cortical connection matrices. Cerebral Cortex 2000;10(2):127–141. [PubMed: 10667981]
6. Honey C, et al. Network structure of cerebral cortex shapes functional connectivity on multiple time scales. PNAS 2007;104(24):10240–10245. [PubMed: 17548818]
7. Gabrieli-Whitfield S, et al. Hyperactivity and hyperconnectivity of the default network in schizophrenia and in first-degree relatives of persons with schizophrenia. PNAS 2009;106(4):1279–1284. [PubMed: 19164577]
8. Burns J, et al. Structural disconnectivity in schizophrenia: A diffusion tensor magnetic resonance imaging study. Br J Psychiatry 2003;182:439–443. [PubMed: 12724248]
9. Ke, M., et al. Combined analysis for resting state fmri and dti data reveals abnormal development of function-structure in early-onset schizophrenia. In: Wang, G.; Li, T.; Grzymala-Busse, JW.; Miao, D.; Skowron, A.; Yao, Y., editors. RSKT 2008. LNCS (LNAI). Vol. 5009. Springer; Heidelberg: 2008. p. 628-635.
10. Zhou Y, et al. Altered resting-state functional connectivity and anatomical connectivity of hippocampus in schizophrenia. Schiz Res 2008;100(1-3):120–132.
11. Jordan M, et al. An introduction to variational methods for graphical models. Machine Learning 1999;37(2):183–233.
12. Fischl B, et al. Sequence-independent segmentation of magnetic resonance images. NeuroImage 2004;23:69–84.
13. Malcolm J, Shenton M, Rathi Y. Neural tractography using an unscented kalman filter. IPMI 2009:126–138.
14. Smith SM, et al. Advances in functional and structural mr image analysis and implementation as fsl. NeuroImage 2004;23(51):208–219.
15. Kubicki M, et al. A review of diffusion tensor imaging studies in schizophrenia. Journal of Psychiatric Research 2007;41(1-2):15–30. [PubMed: 16023676]

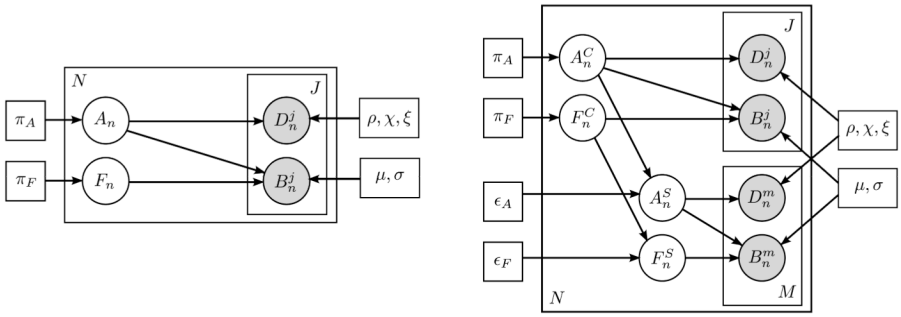

(a) Joint fMRI/DWI model (b) Model of population differences

Fig. 1.

(a) Joint connectivity model for a single population. (b) Joint model for the effects of schizophrenia. The pairwise connections are indexed by $n = 1, \ldots, N$, the control subjects are indexed by $j = 1, \ldots, J$, and the schizophrenia patients are indexed by $m = 1, \ldots, M$. Squares indicate non-random parameters; circles indicate hidden random variables; all shaded variables are observed.

NIH-PA Author Manuscript NIH-PA Author Manuscript NIH-PA Author Manuscript

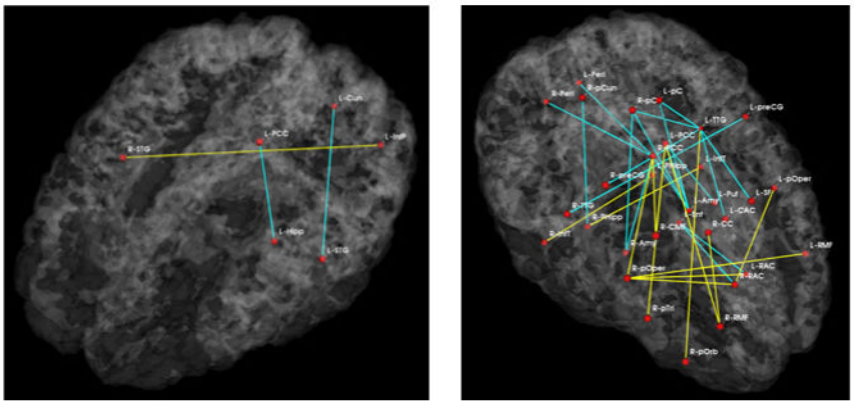

(a) Anatomical Differences (b) Functional Differences

Fig. 2.

Significant anatomical and functional connectivity differences ($p < 0.05$ and $\widehat{\varepsilon}_A^n, \widehat{\varepsilon}_F^n > 0.5$). Blue lines indicate higher connectivity in the control group; yellow lines indicate higher connectivity in the schizophrenia population.

NIH-PA Author Manuscript NIH-PA Author Manuscript NIH-PA Author Manuscript

NIH-PA Author Manuscript
NIH-PA Author Manuscript
NIH-PA Author Manuscript

Table 1

Parameters of the joint model in Fig. 1(a), estimated separately for control (NC) and schizophrenic (SZ) populations, and for the entire dataset (NC+SZ)[1]]

	π_A	$\pi_{F,-1}$	π_{F0}	π_{F1}	ρ_0	ρ_1	χ_0	χ_1	ξ_0	ξ_1		
NC	0.37	0.43	0.40	0.17	0.66	0.10	0.42	0.34	0.005	0.003		
SZ	0.37	0.43	0.41	0.16	0.67	0.11	0.41	0.34	0.005	0.003		
NC+SZ	0.36	0.43	0.40	0.17	0.66	0.11	0.41	0.34	0.005	0.003		
	$\mu_{0,-1}$	$\mu_{1,-1}$	μ_{00}	μ_{10}	μ_{01}	μ_{11}	$\sigma^2_{0,-1}$	$\sigma^2_{1,-1}$	σ^2_{00}	σ^2_{10}	σ^2_{01}	σ^2_{11}
NC	-0.063	-0.022	0.006	0.093	0.12	0.27	0.014	0.010	0.008	0.012	0.019	0.033
SZ	-0.083	-0.036	0.001	0.097	0.13	0.27	0.011	0.011	0.013	0.013	0.017	0.035
NC+SZ	-0.073	-0.027	0.003	0.099	0.12	0.28	0.012	0.011	0.012	0.012	0.017	0.035

[1] $\chi_0 \chi_1$ implies that spurious DWI fibers arise due to artificially high anisotropy.

NIH-PA Author Manuscript

NIH-PA Author Manuscript

NIH-PA Author Manuscript

Table 2
Top 5 significant anatomical (top) and functional (bottom) connections

Region 1	Region 2	p-value	$\widetilde{\varepsilon}_A^n / \widetilde{\varepsilon}_F^n$
R Superior Temporal Gyrus (R-STG)	L Inferior Parietal (L-InfP)	0.0005	0.85
L Posterior Cingulate (L-PCC)	L Hippocampus (L-Hipp)	0.0045	0.79
L Superior Temporal Gyrus (L-STG)	L Cuneus (L-Cun)	0.011	0.93
R Pars Triangularis (R-pTri)	L Posterior Cingulate (L-PCC)	0.0001	0.92
R Paracentral Gyrus (R-pC)	L Transverse Temporal (L-TTG)	0.0001	0.89
L Transverse Temporal (L-TTG)	L Paracentral Gyrus (L-pC)	0.0001	0.55

NIH-PA Author Manuscript

NIH-PA Author Manuscript

NIH-PA Author Manuscript

Table 3

Training and testing accuracy of ten-fold cross validation for the control (NC) and Schizophrenic (SZ) populations

	Training NC	Training SZ	Testing NC	Testing SZ
Joint fMRI/DWI Model	0.99 ± 0.005	0.88 ± 0.01	0.61 ± 0.06	0.55 ± 0.05
linear SVM fMRI	1.00 ± 0.00	1.00 ± 0.00	0.54 ± 0.05	0.61 ± 0.05
linear SVM DWI	1.00 ± 0.00	1.00 ± 0.00	0.59 ± 0.08	0.58 ± 0.06
linear SVM fMRI/DWI	1.00 ± 0.00	1.00 ± 0.00	0.67 ± 0.04	0.60 ± 0.05